

Electron bubbles in helium clusters. I. Structure and energeticsMichael Rosenblit^{a)} and Joshua Jortner^{b)}*School of Chemistry, Tel Aviv University, Ramat Aviv, 69978 Tel Aviv, Israel*

(Received 11 January 2006; accepted 13 March 2006; published online 17 May 2006)

In this paper we present a theoretical study of the structure, energetics, potential energy surfaces, and energetic stability of excess electron bubbles in $({}^4\text{He})_N$ ($N=6500-10^6$) clusters. The subsystem of the helium atoms was treated by the density functional method. The density profile was specified by a void (i.e., an empty bubble) at the cluster center, a rising profile towards a constant interior value (described by a power exponential), and a decreasing profile near the cluster surface (described in terms of a Gudermannian function). The cluster surface density profile width (~ 6 Å) weakly depends on the bubble radius R_b , while the interior surface profile widths ($\sim 4-8$ Å) increase with increasing R_b . The cluster deformation energy E_d accompanying the bubble formation originates from the bubble surface energy, the exterior cluster surface energy change, and the energy increase due to intracluster density changes, with the latter term providing the dominant contribution for $N=6500-2 \times 10^5$. The excess electron energy E_e was calculated at a fixed nuclear configuration using a pseudopotential method, with an effective (nonlocal) potential, which incorporates repulsion and polarization effects. Concurrently, the energy V_0 of the quasi-free-electron within the deformed cluster was calculated. The total electron bubble energies $E_t = E_e + E_d$, which represent the energetic configurational diagrams of E_t vs R_b (at fixed N), provide the equilibrium bubble radii R_b^c and the corresponding total equilibrium energies E_t^c , with $E_t^c(R_e)$ decreasing (increasing) with increasing N (i.e., at $N=6500$, $R_e=13.5$ Å and $E_t^c=0.86$ eV, while at $N=1.8 \times 10^5$, $R_e=16.6$ Å and $E_t^c=0.39$ eV). The cluster size dependence of the energy gap ($V_0 - E_t^c$) allows for the estimate of the minimal $({}^4\text{He})_N$ cluster size of $N \approx 5200$ for which the electron bubble is energetically stable. © 2006 American Institute of Physics. [DOI: 10.1063/1.2192780]

I. INTRODUCTION

Excess electron states in bulk liquid ${}^4\text{He}$ were discovered by Meyer and Reif in their pioneering search for microscopic probes for superfluidity.¹ In their work the Landau-Feynman roton energy^{2,3} was determined from the temperature dependence of the electron mobility in superfluid ${}^4\text{He}$.¹ Most surprising was the moderately low electron mobility (i.e., $\mu \approx 10^{-2}$ cm² V⁻¹ s⁻¹ at $T=2.2$ K,¹) which indicated excess electron localization.⁴⁻⁶ It was demonstrated by Kestner *et al.*,⁴ Jortner *et al.*,⁵ and by Onsager⁶ that the pseudopotential between an electron and a helium atom is strongly short-range repulsive, with a very weak long-range attractive polarization interaction.^{4,7-9} Accordingly, the conduction band energy for a quasi-free-excess-electron in structurally unperturbed bulk liquid He is large and positive, i.e., $V_0=1.06$ eV for ${}^4\text{He}$,^{4,7-18} and $V_0 \approx 0.9$ eV for ${}^3\text{He}$,⁹⁻¹¹ with the conduction band lying above the vacuum level. The direct implications of these high positive energies of the quasi-free-electron state are the exterior and interior localizations of the excess electron. Two distinct types of excess electron states in and on bulk liquid He are manifested, involving the electron exterior surface state^{11,19-27} and the electron interior bubble state.^{5,6,9,10,28-39}

A similar physical situation prevails for excess electron localization on and in $(\text{He})_N$ clusters. The excess electron external surface state, which is stabilized by an image force, was predicted to be realized⁴⁰⁻⁴² above a threshold cluster size N_c and a cluster radius R_c [$N_c=3 \times 10^5$ for $({}^4\text{He})_N$ and $N_c=5.7 \times 10^5$ for $({}^3\text{He})_N$], above which the image potential is sufficiently strong to support a bound ground state, with a binding energy $E_s(R) > E_s(\infty)$ for $R > R_c$, where $E_s(\infty) = -0.74$ meV is the macroscopic surface binding energy. The internal electron bubble state was proposed to be realized in sufficiently large He clusters.^{43,44} The experimental genesis of this field rested on the metastable excitation of large helium clusters by electron impact and on the observation of electron attachment to helium clusters.⁴⁵ Extensive experimental studies^{43,44,46,47} used electron capture to determine the size distributions of very large $({}^4\text{He})_N$ clusters with an average size of $\bar{N}=10^5-10^8$. The significant observation^{43,44} that the negative $(\text{He})_N^-$ cluster ions do not field ionize in electric fields of 10^3 V/cm on a time scale of $50 \mu\text{s}$ seems to rule out the formation of excess electron surface states on these clusters under current experimental conditions. On the basis of these experimental observations, it was proposed⁴⁴ that electron bombardment of $(\text{He})_N$ clusters results in the formation of interior electron bubbles. Further experimental evidence for the formation of interior electron bubbles via electron attachment to large clusters ($N=10^5-10^8$) was reported.⁴⁸ In important experiments⁴⁹⁻⁵¹ dramatic differences were observed for the time scale for the detachment of

^{a)}Present address: Ilse Katz Center for Meso- and Nanoscale Science and Technology, Ben-Gurion University of the Negev, 84105 Beer Sheva, Israel.

^{b)}Electronic mail: jortner@chemsg1.tau.ac.il

electrons from $({}^4\text{He})_N^-$ clusters at 0.37 K and from $({}^3\text{He})_N^-$ clusters at 0.15 K. Electron detachment from $({}^4\text{He})_N^-$ clusters in the size domain of $N=10^5-10^7$ was characterized by lifetimes in the range of $10^{-3}-3\times 10^{-1}$ s,⁴⁷⁻⁵¹ and the cluster size dependence of these lifetimes was established.^{50,51} These lifetimes are shortened by the presence of heavy rare gas impurities.⁴⁹ On the other hand, considerably longer lifetimes were observed for electron detachment from $({}^3\text{He})_N^-$ clusters, which are not amenable to experimental interrogation.⁴⁸⁻⁵¹ These observations were interpreted in terms of the dynamics for the motion of the electron bubble in superfluid $({}^4\text{He})_N^-$ clusters, in contrast to the viscous bubble dynamics in normal fluid $({}^3\text{He})_N^-$ clusters.⁴⁸⁻⁵¹

In view of the fundamental importance of probing collective excitations in finite, interacting boson quantum systems, we present in this paper a theoretical study of electron bubbles in $({}^4\text{He})_N$ clusters. A combination of the density functional method⁵²⁻⁵⁸ for these clusters deformed by a bubble formation, in conjunction with quantum mechanical pseudopotential calculations for the electron-He-atom interactions, was used to describe the electron bubble. We consider a cluster of N ${}^4\text{He}$ atoms of mass m and radius r_0 , together with a single excess electron. The subsystem of the helium atoms was treated by the density functional formalism, while the excess electron was treated quantum mechanically. The energetics and charge distribution of the electron bubble were calculated within the framework of the adiabatic approximation for each fixed nuclear configuration. This study resulted in information on the structure, energetics, and energetic stability of the electron bubble in $({}^4\text{He})_N$ clusters. A preliminary report of our results was already presented.⁵⁹ The structural and energetic information obtained herein will be utilized in the accompanying paper⁶⁰ for the exploration of electron tunneling times from electron bubbles in these clusters, demonstrating that the dynamics of electron tunneling from bubbles in $({}^4\text{He})_N$ clusters will provide a microscopic probe of superfluidity in these finite quantum systems.

II. BUBBLES IN HELIUM CLUSTERS

We first treat the structure and energetics of an empty bubble in the center of a large neutral $({}^4\text{He})_N$ cluster ($N=10^3-10^7$) using the phenomenological density functional approach of Ebner and Saam.⁵² The internal energy E of the nonuniform system was expressed by a functional of the number density $n(\mathbf{r})$ and an expansion in powers of the difference between densities at different points in the system and can be recast in the form⁵²

$$E[n(\mathbf{r})] = \int \epsilon(n(\mathbf{r}))d^3\mathbf{r} + (\hbar^2/2m) \int d^3\mathbf{r}(\nabla n(\mathbf{r}))^2 + F(n(\mathbf{r})). \quad (1)$$

The first term in Eq. (1) represents the energy of the uniform helium system with the energy density $\epsilon(r)$. The second term, with m being the mass of the ${}^4\text{He}$ atom, represents the quantum pressure term,^{39,52,53} and the third term represents the effective interaction that arises from zero-point energy renormalization effects due to the nonuniformity of the system.⁵² The density functional was obtained from Eq. (1)

by neglecting the effective interaction $F(n(r))$ and representing the energy density as a power series in the local density⁵²

$$\epsilon(n) = A_1n^2 + A_2n^3 + A_3n^4. \quad (2)$$

The coefficients $A_i(i=1-3)$ in Eq. (2) are determined by the condition that both the energy density and the chemical potential and compressibility calculated from Eq. (1) in the bulk limit ($N\rightarrow\infty$) correspond to these properties for the macroscopic liquid helium at zero temperature and pressure.^{28,61,62} The power series expansion of the energy density, Eq. (2), yielded an (approximate) analytic solution for an infinite quantum liquid without a bubble.⁵² The density corresponding to the ground state of the system minimizes its total energy and can be obtained from the Euler equation

$$\delta\{E[n(\mathbf{r})] - \mu \int n(\mathbf{r})d^3\mathbf{r}\} = 0, \quad (3)$$

where μ is the chemical potential.⁵² For a spherical helium droplet, Eqs. (1)–(3) result in

$$\mu = -(\hbar^2/2m)(\nabla^2 n(r))^{1/2}/n(r)^{1/2} + 2A_1n(r) + 3A_2n^2(r) + 4A_3n^3(r). \quad (4)$$

This result can be expressed in a dimensionless form

$$\nabla^2 g(x) = g(x)B(x), \quad (5)$$

where

$$B(x) = (a_1g^2(x) + a_2g^4(x) + a_3g^6(x) - \mu/E_v). \quad (6)$$

The function $g(x)$ is defined in terms of the normalized local density

$$g(x) = n^{1/2}(x)/n_0^{1/2}(x), \quad (7)$$

where x is the normalized radius

$$x = r/r_f, \quad (7a)$$

with

$$r_f = (\hbar^2/2mE_v)^{1/2}, \quad (7b)$$

and the coefficients a_i in Eq. (6) are expressed in terms of the parameters A_i , Eq. (2), being given by

$$a_i = (i+1)A_i\bar{n}_0^i/E_v \quad (i=1-3), \quad (8)$$

where \bar{n}_0 is the average number density in the bulk at zero temperature and pressure and E_v is the binding energy per atom in the bulk, which was taken from the experimental data^{28,61-63} as $E_v=0.616$ meV. The coefficients a_i , Eq. (8), are $a_1=-2.2$, $a_2=-2.4$, and $a_3=3.6$.

The internal cluster energy E_c and the number of atoms N in the cluster are given by

$$E_c = 4\pi \int \epsilon_{\text{total}}(n(r))r^2 dr, \quad (9)$$

with

$$\epsilon_{\text{total}}(n(r)) = \epsilon(n(r)) + (\hbar^2/2m)(\nabla n(r))^{1/2}{}^2, \quad (9a)$$

and

$$N = 4\pi \int n(r)r^2 dr. \quad (10)$$

Equations (9) and (10) are applicable both for an ordinary cluster and for a cluster with a bubble. To characterize the density profile for the cluster with a bubble, we choose the helium atom density function in the form of a void at $r < R_b - t_1/2$, a rising profile towards a constant density with increasing r beyond the void boundary at $r > R_b - t_1/2$, and the cluster exterior decreasing density profile for $r > R - t_2/2$. Here R_b is the bubble radius, R is the cluster radius, t_1 is an effective thickness parameter for the density profile of the bubble wall, and t_2 is the thickness of the cluster surface density profile. The explicit form of the helium density profile was taken as

$$n(r) = 0, \quad 0 < r < R_b - t_1/2, \quad (11a)$$

$$n(r) = n_0 [1 - (1 + br) \exp(-b^3 r^3)]^3, \quad (11b)$$

$$R_b - t_1/2 < r < R - t_2/2,$$

$$n(r) = (c) \arctan[\{\sinh(2r/t_2)\}^{-1}], \quad r > R - t_2/2. \quad (11c)$$

The parameter b in Eq. (11b) specifies spatial saturation taking $b = [R_b - t_1/2]^{-1}$. The parameter c in Eq. (11c) is taken as $(c) = (2n_0/\pi)$. n_0 in Eqs. (11b) and (11c) is the asymptotic density is the interior of the cluster. For sufficiently large clusters the density n_0 converges to the bulk value \bar{n}_0 . Equation (11b) was advanced on the basis of previous work on nonuniform ^4He near a hard wall.⁵² Equation (11c) represents the surface density profile of the cluster with a bubble in the form of the Gudermannian function.^{40–42} From a numerical representation of the density profile, Eqs. (11a)–(11c), we assert that t_2 represents the exterior surface profile of the cluster characterized by the 90%–10% fall-off width, while the interior profile of the bubble is characterized by the 10%–90% rise width t_1 . Finally, R_b is the radius of the sphere where $n(r) = n_0/2$.

The density functional approach used above for the energetics of the cluster was applied by us for the cluster with a bubble. It is assumed that $t_1, t_2 < R_b$ and $t_1, t_2 \ll R$, so that nonuniformity effects created by the bubble formation are small. We employed the trial function for the density, Eqs. (11a)–(11c), and for the calculations of $g(x)$, Eq. (7), to compute $B(x)$, Eq. (6), and then to numerically solve Eq. (4). The new density $n(r)$ thus obtained was used to calculate $B(x)$ in a self-consistent procedure. Equations (9) and (10) were then used to calculate the cluster internal energy $E_c(R)$ and the number of particles N for the cluster with a bubble. Calculations of the cluster energy with a bubble $E_c(R_b, R, N)$, Eq. (9), were performed for several, fixed bubble radii R_b with a constant number N of particles. The cluster energies also depend on the exterior and interior density profile thicknesses t_1 and t_2 , respectively, which were varied in the calculations in the range of 4–9 Å to minimize the cluster energy and to keep a fixed number of atoms in the cluster of definite size. The energy of a cluster without a bubble $E_c(R_b=0, R, N)$ was calculated for $R_b=0$ and $t_1=0$, with varying the exterior density profile thickness. The reorgani-

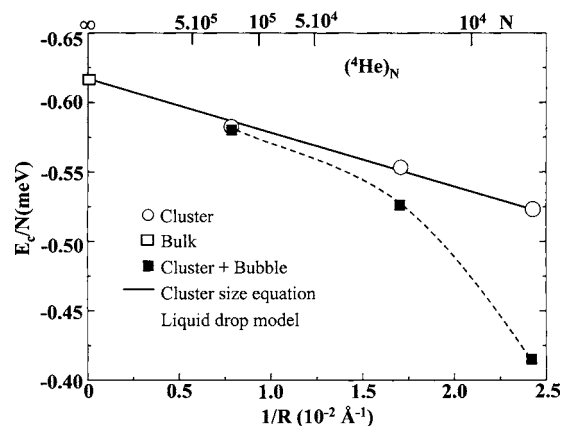


FIG. 1. The cluster size dependence of the calculated binding energies per atom for a $(^4\text{He})_N$ cluster ($N=6.5 \times 10^3 - 1.88 \times 10^5$) of radius R without a bubble (cluster marked as \circ) and for a cluster with a bubble at the equilibrium electron bubble radius R_b (cluster+bubble marked as \blacksquare). The experimental binding energy per atom in the bulk ($R, N=\infty$), $E_c/N = -0.616$ meV ($R, N=\infty$), is also presented (bulk marked as \square). The calculated data for the large clusters ($N=6.5 \times 10^3 - 1.88 \times 10^5$), and the bulk values of E_c/N without a bubble, follow a linear dependence vs $1/R$ and are represented by the liquid drop model with the cluster size equation, Eq. (13) (solid line). The dashed curve connecting the E_c/N data with a bubble was drawn to guide the eye.

zation (deformation) energy $E_d(R_b, R, N)$ of the cluster upon the formation of a bubble of radius R_b at constant N is given by

$$E_d(R_b, R, N) = E_c(R_b, R, N) - E_c(R_b=0, R, N). \quad (12)$$

Calculations of the energetics of bubble formation were performed over a range of cluster sizes ($N=6.5 \times 10^3 - 2 \times 10^5$). Figure 1 portrays the calculated binding energies E_c/N per atom for a ^4He cluster without a bubble, presenting the cluster size dependence of E_c/N per atom for ordinary $(^4\text{He})_N$ clusters in the size domain $N=6.5 \times 10^3 - 2 \times 10^5$. These energies obey the cluster size equation for the liquid drop model^{64–67}

$$E_c/N = E_v + E_s(r_0/R), \quad (13)$$

where $E_v = -0.610$ meV is the volume energy per atom and $E_s = 1.60$ meV is the surface energy per atom. These energetic parameters are in agreement with the experimental value^{28,61–63} $E_v = -0.616$ meV for the atom binding energy in bulk ^4He and with the surface energy $E_s = 1.603$ meV inferred from previous theoretical results⁵⁸ for smaller clusters ($N=128-728$). An additional contribution to E_c/N involves the cluster curvature energy $E_u(r_0/R)^2$ with $E_u = 1.034$ meV. The curvature energy is of importance for small clusters, e.g., $N=128-728$.^{63–66,68,69} The curvature energy term makes only a small contribution to the large clusters studied by us, i.e., for $N=6.5 \times 10^3$ the relative contribution of the curvature energy to the surface energy (E_u/E_s) (r_0/R) is 3%.

In Fig. 1 we also present the energetics of the $(^4\text{He})_N$ cluster with a bubble, at the equilibrium electron bubble radius R_b , inferred (Sec. III) for the electron bubble. These results manifest the marked increase of E_c/N upon bubble formation, which is due to cluster deformation. Typical data were obtained on the bubble radius R_b , the dependence of the cluster deformation energy per atom E_d/N , Eq. (12), the

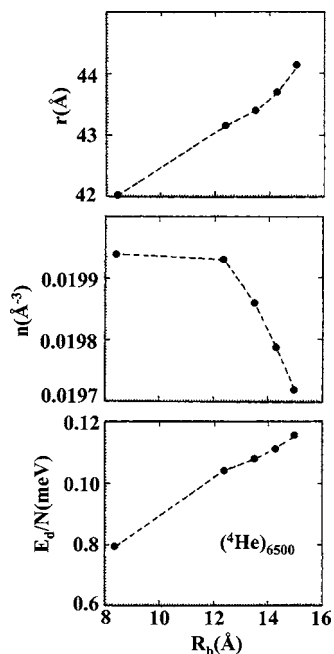
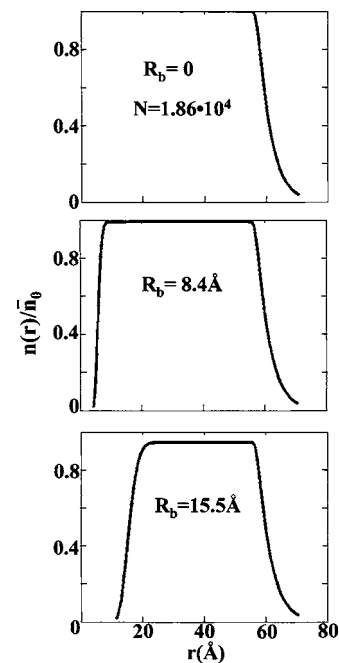


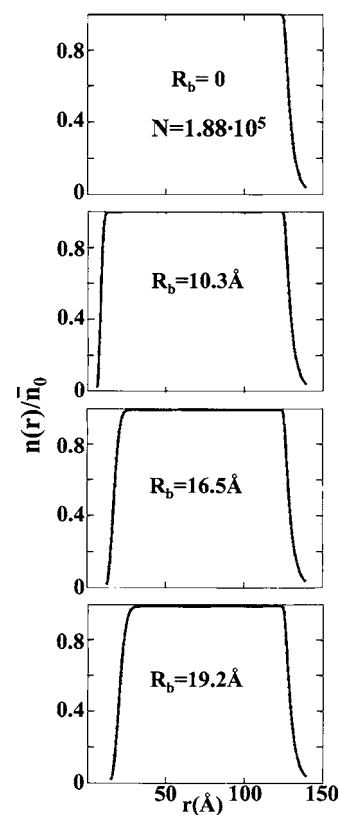
FIG. 2. The dependence on the bubble radius R_b of the cluster reorganization energy E_d/N , of the mean density n , and of the cluster radius R for $N = 6.5 \times 10^3$. These data reflect on the structural manifestations (decrease of n), on the energetic implications (increase of E_d/N), and on the cluster expansion (increase of R) with increasing R_b .

cluster mean density n in the range $R_b + t_1/2 < r < R - t_2/2$, and the cluster radius R for $({}^4\text{He})_N$ clusters (Fig. 2). These results reflect on the energetic implications, i.e., the increase of E_d/N , and on the structural manifestations, i.e., cluster expansion with increasing the bubble radius.

The density profiles for several clusters ($N = 1.86 \times 10^4$ and 1.88×10^5) at different values of the bubble radii R_b are portrayed in Fig. 3. These density profiles reflect on the formation of a “helium balloon” with a finite thickness ($\Delta R \approx R - R_b$) in the cluster, with the center of the bubble being located at the center of the cluster. For clusters without a bubble [Figs. 3(a) and 3(b)], $t_2 = 6.1 \text{ \AA}$ for $N = 1.86 \times 10^4$ and for $N = 1.88 \times 10^5$. The magnitude of t_2 is larger than the value of $t_2 = 4.5 \text{ \AA}$ obtained from variational Monte Carlo simulations for the $({}^4\text{He})_{240}$ cluster⁶⁸ and is close to that inferred from previous density functional calculations for smaller clusters.^{70,71} This value of $t_2 = 6.1 \text{ \AA}$ for the large $N = 1.86 \times 10^4$ and 1.88×10^5 clusters is close to the experimental value⁷² of $t_2 = 7.6_{-2}^{+1} \text{ \AA}$ for bulk liquid ${}^4\text{He}$ at $T = 0 \text{ K}$ and to the theoretical values^{54,55} of $t_2 = 7 \text{ \AA}$ (Ref. 54) and $t_2 = 5.8 \text{ \AA}$ (Ref. 55) for the macroscopic free surface profile. When a bubble with radius R_b is formed in the center of the cluster [Figs. 3(a) and 3(b)], t_2 remains nearly bubble-size independent and close to that for a cluster without a bubble. t_1 exhibits a weak cluster size dependence at fixed R_b and increases with increasing the bubble radius R_b . For $N = 1.86 \times 10^4$, $t_1 = 3.1 \text{ \AA}$ for $R_b = 10 \text{ \AA}$, $t_1 = 6.4 \text{ \AA}$ for $R_b = 15.1 \text{ \AA}$, and $t_1 = 7.9 \text{ \AA}$ for $R_b = 19.0 \text{ \AA}$. For $N = 1.88 \times 10^5$, $t_1 = 4.2 \text{ \AA}$ for $R_b = 10 \text{ \AA}$, $t_1 = 6.7 \text{ \AA}$ for $R_b = 16.5 \text{ \AA}$, and $t_1 = 8.0 \text{ \AA}$ for $R_b = 19.0 \text{ \AA}$. Finally, for $N = 10^6$, $t_1 = 4.2 \text{ \AA}$ for $R_b = 10 \text{ \AA}$, $t_1 = 6.8 \text{ \AA}$ for $R_b = 17 \text{ \AA}$, and $t_1 = 8.0 \text{ \AA}$ for $R_b = 19.0 \text{ \AA}$. As



(a)



(b)

FIG. 3. The density profiles $n(r)/\bar{n}_0(\infty)$, where $\bar{n}_0(\infty)$ is the bulk density, at different bubble radii for $({}^4\text{He})_N$ clusters with $N = 1.86 \times 10^4$ (a) and with $N = 1.88 \times 10^5$ (b), reflecting on the formation of a “helium balloon” with a finite thickness ($\Delta R = R - R_b$) with the bubble center being located at the center of the cluster.

expected, the bubble is more rigid for smaller values of R_b at a fixed cluster size. The bubble surface profile values of the equilibrium electron bubble radius R_b^e (see Sec. III below) are $t_1 = 6.4 \text{ \AA}$ at $R_b^e = 15.1 \text{ \AA}$, $t_1 = 6.7 \text{ \AA}$ at $R_b^e = 16.5 \text{ \AA}$, and

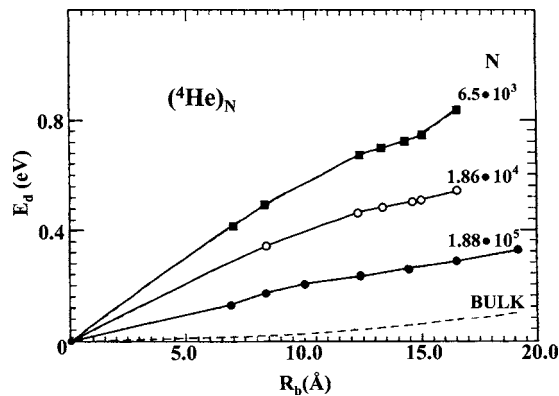


FIG. 4. The dependence of the cluster reorganization energy, Eq. (12), on the radius R_b of the bubble. Data are presented for different cluster sizes N , which are marked on the curves, and for the bulk.

$t_1 = 6.8 \text{ \AA}$ at $R_b^e = 17.0 \text{ \AA}$. These values of t_1 at R_b^e are larger than the values of $t_1 = 4.4 \text{ \AA}$ calculated for the equilibrium configuration of the electron bubble in macroscopic liquid ^4He .⁵⁶ It appears that the bubble at its equilibrium configuration in the cluster is “softer” than in the bulk liquid ^4He .

The energetics of the formation of a helium balloon, i.e., a helium cluster with a bubble at its center (Fig. 4), reveals high reorganization energies, which for $R_b = 13.5 \text{ \AA}$ [corresponding to the value of the equilibrium bubble radius R_b^e for $N = 6500$ (Sec. III)] fall in the range of $E_d = 0.72 \text{ eV}$ for $N = 6.5 \times 10^3$ to $E_d = 0.26 \text{ eV}$ for $N = 1.88 \times 10^5$, increasing with decreasing N at a fixed value of R_b . These E_d values increase with increasing the bubble radius R_b for clusters with a fixed value of N . It is also instructive to note that for the cluster size domain studied herein the E_d values are considerably higher than the bubble formation energy in the bulk $E_d(\infty) \approx 4\pi\gamma R_b^2$, where γ is the surface tension. While the reorganization energy in the bulk is dominated by the bubble surface energy, the reorganization energy for bubble formation in the cluster is determined by three contributions, i.e., the interior bubble surface energy change $E_b(R_b)$, the exterior cluster surface energy $E_c(R)$, and the cluster energy increase due to density changes $\Delta(n(r); N)$. All these three energy contributions are cluster size dependent.

For a rough estimate of the surface energy contributions, we shall use a step function density profile, so that $E_b(R_b) = 4\pi R_b^2 \gamma$ and $E_c(R) = 8\pi\gamma R \Delta R$, where $\Delta R (\ll R)$ is the expansion of the cluster radius upon the formation of the bubble, i.e., $\Delta R = [R(R_b) - R(R_b = 0)]$. Within the framework of this approximate relation we have

$$E_d(R_b, R, N) = 4\pi R_b^2 \gamma + 8\pi\gamma R \Delta R + \Delta(n(r); N). \quad (14)$$

The surface term contributions to E_d in Eq. (14) are moderately small. For example, for $N = 6.5 \times 10^3$ ($R = 43.7 \text{ \AA}$) at the equilibrium bubble radius $R_b = 14.4 \text{ \AA}$, we find from the complete simulations that $E_d = 0.72 \text{ eV}$, while $\Delta R = 2.7 \text{ \AA}$. For this cluster $E_b(R_b) = 5.7 \times 10^{-2} \text{ eV}$ and $E_c(R) = 6.5 \times 10^{-2} \text{ eV}$, with $E_b + E_c = 0.122 \text{ eV}$ providing a contribution of $\sim 16\%$ to the reorganization energy. The dominating contribution to E_d , Eq. (14), for the cluster size domain studied herein, originates from the contribution of the density changes, i.e., the third term in Eq. (14). With increasing the cluster size to-

wards the bulk ($N \rightarrow \infty$), $E_c(R) \rightarrow 0$ and $\Delta(n(r); N) \rightarrow 0$, with $E_d(R_b, R \rightarrow \infty, N \rightarrow \infty) \rightarrow E_b(R_b)$.

III. THE EXCESS ELECTRON BUBBLE

We now introduce an excess electron into the bubble, which is located in the center of the helium cluster, at a fixed nuclear configuration of the “helium balloon.” The electronic energy of the excess electron will be calculated at a fixed nuclear configuration within the Born-Oppenheimer approximation. We modified the nonlocal effective potential developed by us for surface excess electron states on helium clusters^{40–42} for the case of an excess electron in a bubble of radius R_b located in a cluster of radius R . This potential $V(r)$ at distance r from the center of the bubble (and of the cluster) will be subdivided into interior and exterior contributions in the form

$$V(r) = V_{<}(r), \quad r \leq R_b - t_1/2, \quad (15a)$$

$$V(r) = V_{>}(r), \quad r \geq R_b - t_1/2, \quad (15b)$$

where the thickness density profile of the bubble wall is defined by Eqs. (11a)–(11c) and r is the distance from the center of the cluster.

The exterior contribution $V_{>}(r)$ to the potential in Eq. (15b) is determined by the energy of the quasi-free-electron in the finite system being given by^{9,11,18}

$$V_{>}(r) = T + V_p(r), \quad (16)$$

where the repulsive short-range contribution T is represented by the Wigner-Seitz model with a hard-core pseudopotential with radius a , which is taken as the e-He scattering length.^{4–6,9,11,29} The attractive contribution V_p is given as the polarization energy of the cluster, which is induced by the electron within the Wigner-Seitz cell.^{8,9,11,18} The cluster polarization energy is expressed as the sum of the contribution U_p^{in} of the atom inside the Wigner-Seitz cell, the contribution U_p^{out} of the atoms outside the Wigner-Seitz cell in an infinite medium, and the correction term V_p^c to the polarization energy for the finite size of the cluster, due to the excluded volume effect

$$V_p(r) = U_p^{\text{in}} + U_p^{\text{out}} + V_p^c(r, R), \quad (17)$$

where

$$U_p^{\text{in}} = (2\pi\hbar^2/2m_e)na_p, \quad (18)$$

$$U_p^{\text{out}} = -2\pi(4\pi/3)^{1/3}\alpha e^2 n^{4/3}(1 + 8\pi na/3)^{-1}, \quad (19)$$

and

$$V_p^c(r, R) = (e^2/2R)(1 - \varepsilon^{-1}) \sum_{j=0}^{\infty} (j+1)/(j\varepsilon + j+1)(r/R)^{2j}. \quad (20)$$

Here a_p is the e-He scattering length due to the polarization potential, which was taken as¹¹ $a_p = -0.1 \text{ \AA}$, α is the atomic polarizability, and n is the average helium density.

The interior contribution $V_{<}(r)$ to the potential, Eq. (15a), is given by the superposition of electron-atom pseudo-

potentials exerted on the electron by the helium atoms within the surface density profile of the bubble walls and by the electronic polarization potential $V_i(r)$ induced within the region of the bubble, which is represented in terms of a cluster image potential

$$V_{<}(r) = \int_{R_b-t_1/2}^{R_b+t_1/2} d^3r' \nu_{ps}(r'-r)n(r') + V_i(r), \quad (21)$$

where ν_{ps} is the electron-He-atom pseudopotential^{4,5,7-9} and $n(r)$ is the bubble surface density profile, Eq. (11b). The first term in Eq. (21) is the contribution of the polarization potential from the density profile of the bubble. The second term, $V_i(r)$, is the polarization potential induced within the rest of the cluster outside the bubble, which is given by

$$V_i(r) = V_i(r, R) - V_i(r, R_b), \quad (22)$$

where $V_i(r, R)$ is the image potential for a helium cluster of radius R and $V_i(r, R_b)$ is the image potential for the cluster region occupied by a bubble. Equation (22) assumes the form

$$V_i(y) = (e^2/4R)(1/\varepsilon - 1)/(1 + \varepsilon) \times \left[2\beta/(\beta^2 - y^2) - 2/(1 - y^2) + (1/y) \left(\ln \left| \frac{\beta + y}{\beta - y} \right| - \ln \left| \frac{1 + y}{1 - y} \right| \right) \right], \quad (23)$$

where ε is the dielectric constant (taken as that for macroscopic helium), $y=r/R$, and $\beta=R_b/R$.

The potential $V(r)$ is given by the interior contribution $V_{<}(r)$, Eqs. (15a) and (21)–(23), and the exterior contribution $V_{>}(r)$, Eqs. (15b) and (16)–(20). To obtain the ground state electronic energy E_e of the bound excess electron in the bubble at a fixed nuclear configuration we solved numerically the one-electron Schrödinger equation

$$[-(\hbar^2/2m_e)\nabla^2 + V(r) - E_e]\psi(r) = 0, \quad (24)$$

where m_e is the electron mass. The fixed nuclear configuration for an electron bubble in a $({}^4\text{He})_N$ cluster was specified by the cluster radius R , the bubble radius R_b , and the exterior (t_2) and interior (t_1) surface profile parameters. As the electronic energy E_e is smaller than the deformation energy E_d , we assume that changes in the structure of the cluster exterior interface and of the interior diffusiveness of the electron bubble relative to the empty bubble manifest a small effect on E_e . Accordingly, we have chosen t_1 and t_2 as the surface profile parameters for the minimization of the energy of the empty bubble. The parameters N , R , and R_b were varied for the calculation of the electronic energy $E_e(R_b, R, N)$.

The total energy $E_t(R_b, R, N)$ of the electron bubble in a helium cluster is expressed in the form

$$E_t(R_b, R, N) = E_e(R_b, R, N) + E_d(R_b, R, N), \quad (25)$$

where the cluster reorganization energy $E_d(R_b, R, N)$ is given by Eq. (12). The energies $E_t(R_b, R, N)$, $E_e(R_b, R, N)$, and $E_d(R_b, R, N)$ in Eq. (25) are determined by the bubble radius R_b and the cluster radius R , as well as by the density profile parameters t_1 and t_2 , and by the number of atoms N . The

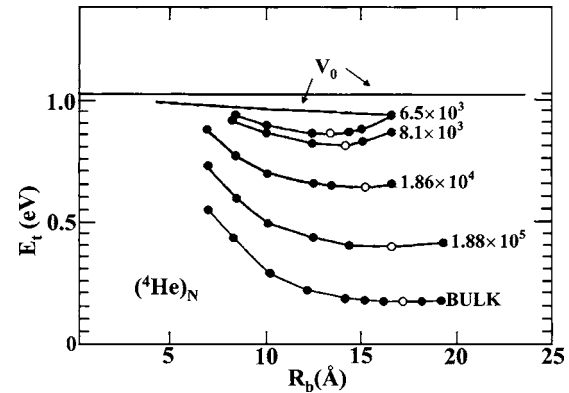


FIG. 5. The potential energy surfaces for the excess electron bubble states in $({}^4\text{He})_N$ clusters portraying the total energy $E_t(R_b, R, N)$ vs the bubble radius R_b for fixed values of N marked on the curves. The full points (●) and open points (○) represent the results of the computations for the clusters using the density functional method for $E_d(R_b, R, N)$ and the quantum mechanical treatment for $E_e(R_b, R, N)$, while for the bulk we took $E_d(R_b, R \rightarrow \infty, N \rightarrow \infty) = 4\pi\gamma R^2$. The open point (○) on each configurational diagram represents the equilibrium radius of the electron bubble. The two straight lines marked V_0 represent the energy of the quasi-free-electron. The horizontal line represents the bulk value of V_0 , while the second line represents $V_0(R_b, R, N)$ in the cluster of the smallest size of $N = 6.5 \times 10^3$. The V_0 values for each R_b for $N = 6.5 \times 10^3 - 1.88 \times 10^5$ fall between these two nearly straight lines.

potential energy surfaces for the excess electron bubble states in ${}^4\text{He}$ clusters in the ground electronic state are portrayed in Fig. 5, where we display $E_t(R_b, R, N)$ vs R_b for fixed values of N . These energetic configurational diagrams exhibit the most stable configuration at their minimal energies at $R_b = R_b^e$, with a total energy E_t^e . The equilibrium electron bubble radii R_b^e and the total energies E_t^e , corresponding to the minima of these potential curves, are presented in Fig. 6. The equilibrium bubble radii (Fig. 6) are $R_b^e = 13.5 \text{ \AA}$ at $N = 6.5 \times 10^3$, $R_b^e = 15.1 \text{ \AA}$ at $N = 1.84 \times 10^4$,

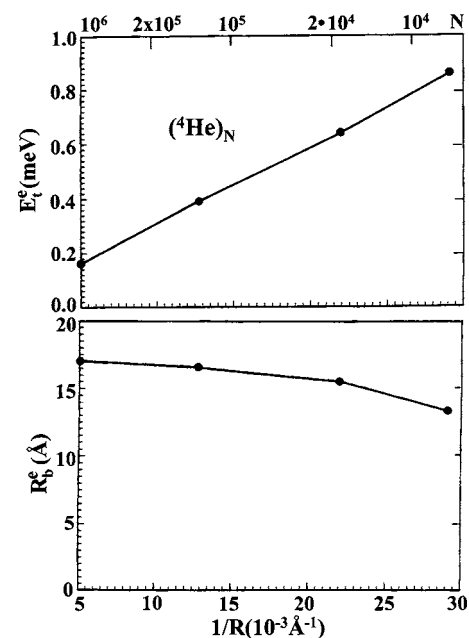


FIG. 6. The cluster size dependence of the equilibrium electron bubble radii R_b^e and the total ground state energies E_t^e , corresponding to the minima of the potential curves of Fig. 5.

$R_b^e = 16.6 \text{ \AA}$ at $N = 1.88 \times 10^5$, and $R_b^e = 17.0 \text{ \AA}$ at $N = 10^6$, increasing with increasing N . The equilibrium electron bubble radius in the largest cluster studied herein, i.e., $R_b^e = 17.0 \text{ \AA}$ for $N = 10^6$ ($R = 222 \text{ \AA}$), converges to the bubble radius in macroscopic liquid ^4He , which was experimentally determined to be $R_b^e = 17.2 \pm 0.15 \text{ \AA}$,⁷³ in accord with theoretical calculations^{8,9,29,37,39,56} that yielded $R_b^e = 17\text{--}18 \text{ \AA}$. The electronic energies at R_b^e are $E_e^e = 0.160 \text{ eV}$ for $N = 6.5 \times 10^3$, $E_e^e = 0.126 \text{ eV}$ for $N = 1.86 \times 10^4$, $E_e^e = 0.102 \text{ eV}$ for $N = 1.88 \times 10^5$, and $E_e^e = 0.08 \text{ eV}$ for $N = 10^6$. The increase of E_e with decreasing the cluster size is due to the increase of R_b^e with increasing N . The electron bubble electronic energy at the equilibrium bubble configuration for the largest cluster studied herein, i.e., $E_e^e = 0.08 \text{ eV}$ for $N = 10^6$, is close to the values of the electronic energy in the range of $0.07\text{--}0.08 \text{ eV}$ calculated^{37,58} for the bubble in macroscopic liquid ^4He . The total energy E_t^e at the equilibrium configuration (Fig. 6) decreases nearly linearly from $E_t^e = 0.86 \text{ eV}$ for $N = 6.5 \times 10^3$ to $E_t^e = 0.38 \text{ eV}$ for $N = 1.88 \times 10^5$. To complete the presentation of the energetic parameters we also present in Fig. 5 the R_b dependence of the energy of the quasi-free-electron state $V_0(R_b^e, R, N)$ in clusters of different sizes, which were calculated using the exterior potential given by Eqs. (16)–(20). These V_0 values in clusters are reduced by less than 10% relative to the bulk values. For the smallest cluster with $N = 6.5 \times 10^3$ studied herein $V_0 = 0.95 \text{ eV}$, for $N = 1.88 \times 10^5$ we have $V_0 = 1.02 \text{ eV}$, while the bulk value is $V_0 = 1.06 \text{ eV}$ (Fig. 1). This reduction of V_0 originates from the lowering of the density within the cluster as compared to the bulk value [Figs. 3(a) and 3(b)]. These energetic data will now be applied to assess the energetic stability of the electron bubble.

IV. THE ENERGETIC STABILITY OF THE ELECTRON BUBBLE

The energy of the excess electron bubble in the ground electronic state at its equilibrium bubble radius R_b^e , with the corresponding cluster radius R^e , is determined by the contributions of the electronic energy and the cluster reorganization energy. The total energy at equilibrium configuration, $E_t(R_b^e, R^e, N)$, is positive relative to the vacuum level, while for a broad range of cluster sizes this energy is lower than the cluster conduction band energy. The equilibrium energy of an electron bubble increases with decreasing N and at some value of N it will become higher than V_0 , marking the onset of the energetic instability of the electron bubble. A central question is what the minimal cluster size is for which the electron bubble is energetically stable. The energetic stability condition for the excess electron bubble state (i.e., an electron in “helium balloon”) is given by

$$E_t^e(R_b^e, R^e, N) \leq V_0(R_b^e, R^e, N). \quad (26)$$

In Fig. 7 we present the plot of $V_0(R_b^e, R^e, N) - E_t^e(R_b^e, R^e, N)$ vs $1/R^e$. An extrapolation of this linear dependence to $V_0 - E_t^e = 0$ (Fig. 7) results in the energetic localization threshold at the cluster equilibrium radius $R^e \leq 39 \text{ \AA}$ of a cluster which contains an electron bubble. For such a cluster, the energetic localization threshold is manifested for $N = [(R^e)^3 - (R_b^e)^3]/r_0^3$, where R_b^e is the equilibrium radius of the electron bubble,

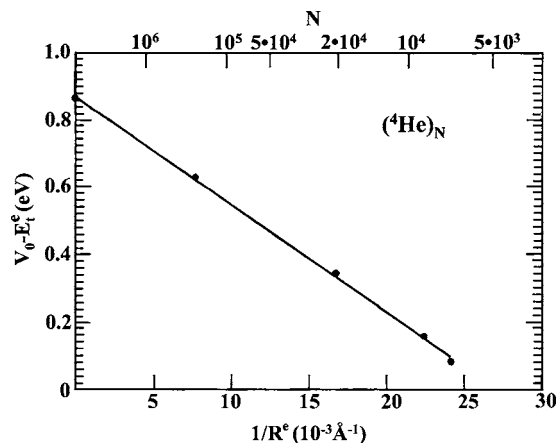


FIG. 7. The dependence of the energy gap ($V_0 - E_t^e$) between the quasi-free-electron energy and the total ground state energy at the equilibrium configuration of the electron bubble on the reciprocal value of the cluster radius at this equilibrium configuration $1/R^e$ for clusters in the range of $N = 6.5 \times 10^3\text{--}1.86 \times 10^4$ and for the bulk. A crude extrapolation of this linear dependence of $V_0 - E_t^e$ to zero leads to a localization threshold at $R \leq 39 \text{ \AA}$, which corresponds to $N \approx 5 \times 10^3$.

which assumes the value $R_b^e \approx 13.5 \text{ \AA}$ in this cluster size domain. Accordingly, we estimate that $N \approx 5200$ for the minimal cluster size for which the electron bubble is energetically stable. This energetic localization threshold constitutes an upper limit for the cluster size, which allows for the existence of the electron bubble state. Dynamic effects, due to electron tunneling of the excess electron from the bubble to the vacuum, may result in the depletion of the energetically stable excess electron bubble state on the experimental time scale for the interrogation of $(\text{He})_N^-$ clusters ($1\text{--}10^{-6} \text{ s}$).^{48–51} Accordingly, the dynamic stability of the excess electron bubble state in $(^4\text{He})_N$ clusters on the experimental time scale may be realized for cluster sizes which are lower than those dictated by the energetic stability. The dynamic stability of the excess electron bubble will be explored in the accompanying paper.⁶⁰

V. DISCUSSION

We explored the structure, energetics, and energetic stability of electron bubbles in large $(^4\text{He})_N$ clusters ($N = 6.5 \times 10^3\text{--}10^7$). The energetics and structure of the electron bubble, which pertain to the deformation energy for the bubble formation, the ground state energy of the localized excess electron, the total energy, and the equilibrium nuclear configuration, are insensitive to the properties of the superfluid, being nearly identical for $(^4\text{He})_N$ normal fluid clusters above the lambda point ($T > T_\lambda$) and for $(^4\text{He})_N$ superfluid clusters (at $T < T_\lambda$). The localization dynamics from the quasi-free-electron state to the localized electron bubble state in a $(^4\text{He})_N$ cluster,^{59,74} which corresponds to intracluster ultrafast dynamics on the time scale of nuclear motion, exhibits rather small effects of superfluidity on the lifetime τ_b for the formation of the equilibrium electron bubble configuration. These superfluidity effects originate from medium dissipation accompanying the electron bubble expansion and depend on the medium viscosity,⁷⁴ which is drastically different for the normal fluid cluster and for the superfluid

cluster.^{58,59,62} The viscosity is finite for normal fluid clusters and is vanishingly small for superfluid clusters.^{58,62} We estimated the following values of bubble formation times for the (${}^4\text{He}$)_N ($N=1.88 \times 10^5$) cluster at $T=0.4$ K: $\tau_b=3.6$ ps without dissipation and $\tau_b=7.8$ ps when medium dissipation was taken into account.^{59,74} We thus expect a decrease of τ_b by a numerical factor of ~ 2 in the superfluid cluster relative to the normal cluster, which originates from the switching off of dissipation effects in the former case. On the time scale of $t > \tau_b$ electron tunneling from the bubbles in (${}^4\text{He}$)_N clusters is grossly affected by the motion of the electron bubble within the cluster,^{48–51,59} which is dissipative in normal fluid (${}^4\text{He}$)_N clusters (at $T > T_\lambda$) and (${}^3\text{He}$)_N clusters (at all temperatures), and nondissipative in superfluid ($T < T_\lambda$) (${}^4\text{He}$)_N clusters. These distinct features of motional bubble dynamics allow for the utilization of electron tunneling from bubbles as a probe for superfluidity in (${}^4\text{He}$)_N clusters.^{48–51,59,60}

Note added in proof. Our values of $t_1=6.4\text{--}6.8$ Å for the bubble profile in clusters are in reasonable agreement with the recent result of $t_1=6.1$ Å reported by V. Grau, M. Barranco, R. Mayol, and M. Pi [Phys. Rev. B **73**, 064502 (2006)] from density functional calculations for the electron bubble in bulk liquid ${}^4\text{He}$.

ACKNOWLEDGMENTS

We are indebted to Professor Milton W. Cole and Professor J. Peter Toennies for their comments on the manuscript. This research was supported by the German-Israeli James Franck Program on Laser-Matter Interaction.

¹L. Meyer and F. Reif, Phys. Rev. **119**, 1164 (1960).

²L. Landau, J. Phys. (USSR) **5**, 71 (1941).

³R. P. Feynman, Phys. Rev. **90**, 116 (1963); **91**, 1291 (1953); **91**, 1301 (1953); **94**, 262 (1954).

⁴N. Kestner, J. Jortner, M. H. Cohen, and S. A. Rice, Phys. Rev. **A56**, 140 (1965).

⁵J. Jortner, S. A. Rice, and N. R. Kestner, in *Modern Quantum Chemistry, Istanbul Lectures*, edited by O. Sinanoglu (Academic, New York, 1965), Vol. II, p. 129.

⁶L. Onsager, in *Modern Quantum Chemistry, Istanbul Lectures*, edited by O. Sinanoglu (Academic, New York, 1965), Vol. II, p. 123.

⁷M. V. Rama Krishna and K. B. Whaley, Phys. Rev. B **38**, 11839 (1988).

⁸B. R. Springett, J. Jortner, and M. H. Cohen, J. Chem. Phys. **48**, 2720 (1968).

⁹J. Jortner, N. Kestner, M. H. Cohen, and S. A. Rice, J. Chem. Phys. **43**, 2614 (1965).

¹⁰K. Hiroiki, N. Kestner, S. A. Rice, and J. Jortner, J. Chem. Phys. **43**, 2625 (1965).

¹¹E. Cheng, M. W. Cole, and M. H. Cohen, Phys. Rev. B **50**, 1136 (1994); **50**, 16134 (1994).

¹²B. Space, D. Coker, Z. Liu, B. J. Berne, and G. Martyna, J. Chem. Phys. **97**, 2002 (1992).

¹³W. T. Sommer, Phys. Rev. Lett. **12**, 271 (1964).

¹⁴M. A. Woolf and G. W. Rayfield, Phys. Rev. Lett. **15**, 235 (1965).

¹⁵J. R. Broomall, W. D. Johnson, and D. G. Onn, Phys. Rev. B **14**, 02819 (1976).

¹⁶B. Plenkiewicz, P. Plenkiewicz, and J. P. Jay-Garin, Chem. Phys. Lett. **178**, 542 (1989).

¹⁷K. Martini, J. P. Toennies, and C. Winkler, Chem. Phys. Lett. **178**, 429 (1991).

¹⁸N. Schwenter, E. E. Koch, and J. Jortner, *Electronic Excitation in Condensed Rare Gases* (Springer, Berlin, 1985).

¹⁹M. W. Cole and M. H. Cohen, Phys. Rev. Lett. **23**, 1238 (1969).

²⁰M. W. Cole, Phys. Rev. B **2**, 4239 (1970).

²¹M. W. Cole, Phys. Rev. B **3**, 4418 (1971).

²²V. B. Shikin, Sov. Phys. JETP **31**, 936 (1970).

²³M. W. Cole, Rev. Mod. Phys. **46**, 451 (1974).

²⁴V. S. Edelman, Sov. Phys. Usp. **23**, 227 (1980).

²⁵J. P. Hernandez, Rev. Mod. Phys. **63**, 675 (1991).

²⁶P. Leiderer, J. Low Temp. Phys. **87**, 247 (1992).

²⁷F. G. Saville, J. M. Goodkind, and P. M. Platzman, Phys. Rev. Lett. **70**, 1517 (1993).

²⁸A. L. Fetter, in *The Physics of Liquid and Solid Helium*, edited by K. H. Benneman and J. B. Ketterson (Wiley, New York, 1976), Pt. 1, p. 207.

²⁹B. R. Springett, J. Jortner, and M. H. Cohen, Phys. Rev. **159**, 183 (1967).

³⁰J. A. Northby and T. M. Sanders, Phys. Rev. Lett. **18**, 1184 (1967).

³¹T. Miyakawa and D. L. Dexter, Phys. Rev. A **1**, 513 (1970).

³²C. C. Grimes and G. Adams, Phys. Rev. B **41**, 6366 (1990); **45**, 2305 (1992).

³³A. Ya. Parshin and V. Pereverzev, Sov. Phys. JETP **74**, 68 (1992).

³⁴W. B. Fowler and D. L. Dexter, Phys. Rev. **176**, 337 (1968).

³⁵W. Schoepe and G. W. Rayfield, Phys. Rev. A **7**, 2111 (1973).

³⁶M. H. Cohen and J. Jortner, Phys. Rev. **180**, 238 (1969).

³⁷Y. M. Shih and C. W. Woo, Phys. Rev. Lett. **30**, 478 (1973).

³⁸K. W. Schwarz, Adv. Chem. Phys. **33**, 1 (1975).

³⁹T. C. Padmore and M. W. Cole, Phys. Rev. A **9**, 802 (1974).

⁴⁰M. Rosenblit and J. Jortner, J. Chem. Phys. **101**, 3029 (1994).

⁴¹M. Rosenblit and J. Jortner, Phys. Rev. B **52**, 17461 (1995).

⁴²M. Rosenblit and J. Jortner, J. Chem. Phys. **101**, 9982 (1994).

⁴³T. Jiang, C. Kim, and J. A. Northby, Phys. Rev. Lett. **71**, 700 (1993).

⁴⁴J. A. Northby, C. Kim, and T. Jian, Physica B **197**, 426 (1994).

⁴⁵J. Gspann, Physica B **169**, 519 (1991).

⁴⁶J. A. Northby, J. Chem. Phys. **115**, 10065 (2001).

⁴⁷K. Martini, J. P. Toennies, and C. Winkler, Chem. Phys. Lett. **178**, 429 (1991).

⁴⁸U. Henne and J. P. Toennies, J. Chem. Phys. **108**, 9327 (1998).

⁴⁹M. Farnik, B. Samelin, and J. P. Toennies, J. Chem. Phys. **110**, 9195 (1999).

⁵⁰M. Farnik, U. Henne, B. Samelin, and J. P. Toennies, Phys. Rev. Lett. **81**, 3892 (1998).

⁵¹M. Farnik and J. P. Toennies, J. Chem. Phys. **118**, 4176 (2003).

⁵²C. Ebner and W. F. Saam, Phys. Rev. B **12**, 923 (1975).

⁵³E. P. Gross, Nuovo Cimento **20**, 454 (1961); J. Math. Phys. **4**, 195 (1963); D. Amit and E. P. Gross, Phys. Rev. **145**, 130 (1966).

⁵⁴S. Stringari and J. Treiner, Phys. Rev. B **36**, 8369 (1987).

⁵⁵J. Dupont-Roc, M. Mimbret, N. Pavloff, and J. Treiner, J. Low Temp. Phys. **81**, 31 (1990).

⁵⁶F. Ancilotto and F. Toigo, Phys. Rev. B **50**, 12820 (1994).

⁵⁷V. R. Pandharipande, S. C. Pieper, and D. M. Ceperly, Phys. Rev. B **34**, 4571 (1990).

⁵⁸F. Dalfovo and S. Stringari, J. Chem. Phys. **115**, 10078 (2001).

⁵⁹J. Jortner and M. Rosenblit, Adv. Chem. Phys. **132**, 247 (2005).

⁶⁰M. Rosenblit and J. Jortner, J. Chem. Phys. **124**, 194506 (2006), following paper.

⁶¹J. Wilks, *Liquid and Solid Helium* (Oxford University Press, Oxford, 1967).

⁶²J. Wilks and D. S. Betts, *An Introduction to Liquid Helium* (Oxford University Press, New York, 1987).

⁶³F. Dalfovo and S. Stringari, J. Chem. Phys. **115**, 10078 (2001).

⁶⁴V. H. Pandharipade, J. G. Zabolinsky, S. C. Pieper, R. B. Wiringa, and U. Helmbrecht, Phys. Rev. Lett. **50**, 1676 (1983).

⁶⁵S. C. Pieper, R. B. Wiringa, and V. R. Pandharipande, Phys. Rev. B **32**, 3341 (1985).

⁶⁶V. R. Pandharipande, S. C. Pieper, and R. B. Wiringa, Phys. Rev. B **34**, 4571 (1986).

⁶⁷J. Jortner, Z. Phys. D: At., Mol. Clusters **24**, 247 (1992).

⁶⁸M. V. Rama Krishna and K. B. Whaley, J. Chem. Phys. **93**, 746 (1990).

⁶⁹S. A. Chin and E. Krotscheck, Phys. Rev. B **52**, 10405 (1995).

⁷⁰S. A. Chin and E. Krotscheck, Phys. Rev. B **45**, 852 (1992).

⁷¹M. V. Rama Krishna and K. B. Whaley, Mod. Phys. Lett. B **4**, 895 (1990).

⁷²L. B. Lurio, T. A. Rabedeau, P. S. Pershan, I. F. Silvera, M. Deutch, S. D. Kosowsky, and B. M. Ocko, Phys. Rev. Lett. **68**, 2628 (1992); **72**, 309(E) (1994).

⁷³J. P. Poirinaud and F. I. B. Williams, Phys. Rev. Lett. **29**, 1230 (1972); **32**, 1213(E) (1974).

⁷⁴M. Rosenblit and J. Jortner, J. Phys. Chem. A **101**, 751 (1997).